Investigating the Performance of Voltage Regulation and Power Smoothing Techniques in MV-LV Distribution Networks

Georgios C. Kryonidis
Dept. of Electr. & Comput. Eng.
Aristotle University of Thessaloniki
Thessaloniki, Greece
kryonidi@ece.auth.gr

Kalliopi D. Pippi
Dept. of Electr. & Comput. Eng.
Democritus University of Thrace
Xanthi, Greece
kpippi@ee.duth.gr

Angelos I. Nousdilis
Dept. of Electr. & Comput. Eng.
University of Western Macedonia
Kozani, Greece
a.nousdilis@uowm.gr

Theofilos A. Papadopoulos
Dept. of Electr. & Comput. Eng.
Democritus University of Thrace
Xanthi, Greece
thpapad@ee.duth.gr

***Abstract*—This paper presents a comparative analysis of the most well-established control strategies for voltage regulation (VR) and power smoothing (PS) in distribution grids with distributed renewable energy sources and battery energy storage systems (DBESSs). The main scope of this analysis is to assess the concurrent operation of VR and PS techniques in terms of voltage violation mitigation, DBESS utilization, smoothing capability, etc. The examined control schemes are applied in distribution networks consisting of sub-grids with different voltage levels, i.e., medium-voltage (MV) and low-voltage (LV), to investigate potential interactions between them. Quasi-static simulations are performed on a MV-LV distribution network consisting of the 33-bus MV benchmark network and the IEEE European LV test feeder, revealing a strong VR interaction between LV and MV sub-grids. Moreover, the concurrent operation of VR and PS techniques improves the VR efficacy by means of reducing the required reactive power at the expense of DBESS utilization.**

***Index Terms*—Battery energy storage systems, distributed generation, power smoothing techniques, voltage regulation, voltage unbalance mitigation.**

I. Introduction

A. Motivation and Background

The proliferation of distributed renewable energy sources (DRESs) has brought to the surface a series of technical challenges that distribution system operators (DSOs) should address to ensure the secure and reliable grid operation [1]. The root cause lies on the reverse power flow due to the active power injection of DRESs and the intermittent nature of their primary energy sources, e.g., wind and solar irradiation. The former can lead to overvoltages, contributing also to the increase of voltage unbalances due to the connection of single-phase DRESs; the latter introduces uncertainty towards the planning and real-time operation of the grid. To overcome these issues, several voltage regulation (VR) and power smoothing (PS) techniques have been proposed in the literature combining DRESs with distributed battery energy storage systems (DBESSs) [2].

The research work was supported by the Hellenic Foundation for Research and Innovation (H.F.R.I.) under the "First Call for H.F.R.I. Research Projects to support Faculty members and Researchers and the procurement of high-cost research equipment grant" (Project Number: HFRI-FM17-229).

B. Relevant Literature

Considering VR, a promising solution is to adopt data-driven control schemes where the output power of each DRES/DBESS is determined by using local and/or remote information [3]–[6]. Specifically, the authors in [3] propose a consensus algorithm to regulate the network voltages by controlling only the active power of DBESSs. In [4], the use of active power is supplemented by considering also the available reactive power of DRESs towards VR of distribution grids. This is attained by introducing controllable $Q(V)$-$P(V)$ droop curves which are coordinated by applying a consensus-based distributed control scheme. In [5], voltage unbalance mitigation (VUM) is included as an additional operating objective in the VR process. In particular, the damping conductance concept is introduced combined with a $P(V)$ droop curve to tackle potential overvoltages. In [6], an enhanced VR method is proposed which is characterized by low computational complexity, leading also to improved DBESS utilization and reduced network losses. The proposed solution is implemented in the symmetrical components domain to avoid potential interactions between VUM and under-/over-voltage mitigation, which is also compliant with the requirements posed by the IEEE 1547 Standard [7].

Regarding PS techniques, DBESSs are used to cover the mismatch between the power injected from the primary energy source and the smoothed power provided to the grid. The

Citation information, DOI: 10.1109/SEST57387.2023.10257495

most well-established PS techniques in the literature can be classified into the filtering algorithms (FAs) and the ramp-rate limitation (RRL) control schemes [8]. In the first category, DBESS absorbs the high frequency power components of the primary energy source which can be calculated by employing one of the following filtering methods: moving-average (MA) [9], low-pass filtering (LPF) [10], high-pass filtering [11], etc. In the second category, DBESS is employed to saturate the DRES power injected to the grid when the ramp-rate of the primary source exceeds a predefined limit [12]. An enhanced version of [12] is proposed in [13] where a feedback control strategy is integrated to the RRL method to ensure that the state-of-charge (SoC) of the DBESS returns back to a predefined set-point.

Based on the above, it can be deduced that most of the methods proposed in the literature address a specific type of problem, e.g., VR, PS, etc., without evaluating their concurrent operation. An initial attempt was made in a previous work [14], where the concurrent provision of VR and PS is investigated. However, a thorough analysis of the network performance is missing, since it mainly focuses on evaluating the DBESS degradation. Additionally, a single level distribution grid is considered, i.e., the IEEE European low-voltage (LV) test feeder [15], neglecting possible interactions that may occur due to the application of these control schemes in distribution networks consisting of sub-grids with different voltage levels, i.e., medium-voltage (MV) and LV (MV-LV).

A few studies deal with the application of control algorithms in MV-LV distribution networks [16]–[18]. In particular, a centralized, optimization-based approach is proposed in [16] for the provision of reactive power support and VR to the transmission system. A coordinated control scheme is proposed in [17], where the on-load tap changer and photovoltaic (PV) curtailment are used as the main control means for VR and congestion management of MV-LV distribution networks. Finally, in [18], an optimization-based conservation voltage reduction method is proposed to minimize the overall energy consumption of a MV-LV distribution network. However, the above-mentioned solutions require detailed network modeling, hindering their application under real-field conditions.

C. Contributions

The scope of this work is twofold: (a) to investigate the operation of the most well-established VR and PS control strategies within a multi-services perspective and (b) to evaluate their performance in MV-LV distribution networks. Contrary to [16]–[18], data-driven VR control strategies are used, since they are network-agnostic and are characterized by low computational complexity. The performance of the examined control scheme is assessed via quasi-static simulations on a benchmark MV-LV distribution network in terms of voltage violation mitigation, DBESS utilization, etc.

II. Data-Driven Control Schemes

In this section, the examined data-driven control schemes are briefly presented.

A. VR Control Strategies

Two types of VR control strategies are considered, namely the proportional and the proportional-integral controls, that are analyzed below. Note that, both VR methods aim at controlling the positive-sequence network voltages as imposed by the IEEE 1547 Standard [7].

1) Proportional control (PC): In this case, the output power of each DRES/DBESS is proportionally adjusted with respect to the positive-sequence voltage at the point of interconnection (POI) with the grid. A profound example of proportional control is the $Q(V)$ and $P(V)$ piecewise droop control schemes that have been widely used for VR studies in distribution grids. In this paper, the combined $Q(V)-P(V)$ droop control scheme of [14] is adopted, which is a modified version of [4] in terms of replacing DRES curtailment with the storage capability of DBESSs.

2) Proportional-integral control (PIC): The key component of this VR control strategy is the introduction of a proportional-integral controller. Scope of this controller is to determine the output power of the DRES/DBESS that eliminates the difference between the actual measured POI voltage and a reference value. This solution is usually combined with a central controller that coordinates the DRES/DBESS to achieve system-wide objectives, e.g., minimization of network losses. In this paper, the solution presented in [6] is adopted.

It is worth mentioning that in both solutions, the DBESS control is supplemented with a day-ahead planning algorithm following the analysis presented in [6] to ensure the availability of the DBESS in the VR process of the next day. Moreover, both solutions respect the technical limits of DRES/DBESS, i.e., the maximum active and reactive power that each DRES/DBESS can exchange with the grid.

B. VUM Techniques

The main idea behind VUM is to reallocate the output power of each DRES/DBESS among the three phases in order to reduce the asymmetry of the POI voltage, which, in turn, leads to a reduction of the voltage asymmetries in the whole network. It is evident that this solution can be only applied to DRESs/DBESSs with three-phase configuration. Two types of VUM techniques are examined, i.e., the damping conductance and the susceptance control schemes, that are described below:

1) Damping conductance control (DCC): In this case, the DRES/DBESS injects negative- and zero-sequence currents that are proportional to the negative- and zero-sequence POI voltages, respectively; thus, operating as a virtual conductance [5]. The value of the damping conductance is determined with respect to the POI voltage following a droop-based control scheme. This solution is also combined with a $P(V)$ droop control scheme to avoid potential overvoltages.

2) Damping susceptance control (DSC): Contrary to the solution proposed in [5], the DRES/DBESS operates as a virtual susceptance by reallocating only the output reactive power among the three phases [6]. This enables the DRES/DBESS to contribute to the VUM of the network, irrespective of the availability of the primary energy source and DBESS.

C. PS Algorithms

Three well-established PS techniques are considered, namely the RRL, the MA, and LPF algorithms, that are briefly presented below. Note that, a thorough analysis of the examined PS techniques is presented in [19].

1) RRL algorithm: Assuming a given time instant t, this algorithm consists of two main steps. The first step deals with the ramp-rate calculation which is defined as $\Delta P/\Delta\tau$. Here, ΔP is the difference between the maximum power point (MPP) of the DRES primary source at the current time instant (P^{t}_{MPP}) and the DRES output power of the previous time instant ($P^{t-\Delta\tau}_{\mathrm{DRES}}$). The second step determines the smoothed DRES active power injected to the grid at time instant t (P^{t}_{DRES}). Specifically, in case the calculated ramp-rate exceeds the permissible limits, i.e., $RR_{\min}$ or $RR_{\max}$, P^{t}_{DRES} is saturated and is set equal to $P^{t-\Delta\tau}_{\mathrm{DRES}}+RR_{\min}\Delta\tau$ or $P^{t-\Delta\tau}_{\mathrm{DRES}}+RR_{\max}\Delta\tau$, respectively. Otherwise, no saturation is applied and P^{t}_{DRES} is set equal to P^{t}_{MPP}.

2) MA algorithm: This is a FA-based solution where the DRES output power at time instant t (P^{t}_{DRES}) is calculated by averaging the corresponding MPP values within a predefined moving window ($N\Delta\tau$) as follows:

$$P^{t}_{\mathrm{DRES}}=\frac{1}{N}\sum_{i=0}^{N}P^{t-i\Delta\tau}_{\mathrm{MPP}} \tag{1}$$

where N stands for the number of the samples preceding time instant t.

3) LPF algorithm: This constitutes an alternative FA-based solution where a discrete implementation of the first-order LPF is used to smooth the DRES output power at time instant t as follows:

$$P^{t}_{\mathrm{DRES}}=\frac{2T_{\mathrm{lpf}}-\Delta\tau}{2T_{\mathrm{lpf}}+\Delta\tau}P^{t-\Delta\tau}_{\mathrm{DRES}}+\frac{\Delta\tau}{2T_{\mathrm{lpf}}+\Delta\tau}(P^{t}_{\mathrm{MPP}}+P^{t-\Delta\tau}_{\mathrm{MPP}}) \tag{2}$$

where T_{lpf} is the time constant of the LPF.

As a common characteristic, all the above PS algorithms are enhanced with the SoC recovery mechanism proposed in [13] to ensure that the energy stored in the DBESS returns back to a predefined set-point ($E^{\mathrm{ref}}_{\mathrm{DBESS}}$) after the PS is finished. Assuming a given time instant t, this is attained by subtracting the term $k\left(E^{\mathrm{ref}}_{\mathrm{DBESS}}-E^{t}_{\mathrm{DBESS}}\right)$ from P^{t}_{MPP} and forwarding it to the corresponding PS algorithm. Here, E^{t}_{DBESS} stands for the stored energy of the DBESS at time instant t and k is a proportional gain.

III. System Under Study

To assess the performance of the data-driven control schemes, quasi-static simulations are conducted on the MV-LV distribution network depicted in Fig. 1 using OpenDSS and MATLAB [20], [21]. The former is used as an unbalanced power flow solver and the latter is utilized for the modeling of data-driven control schemes. The network is composed of two benchmark sub-grids, i.e., the 12.66 kV, 33-bus MV network of [22] and the IEEE 0.4 kV European LV test feeder of [15], which are connected via a 12.66/0.4 kV transformer with a

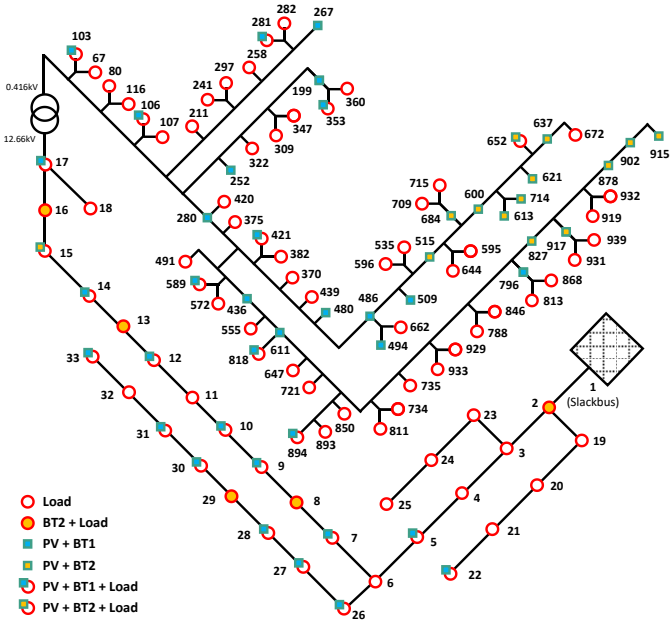

Fig. 1. Single-line diagram of the examined MV-LV network.

rated power of 800 kVA, short-circuit voltage of 4 %, and full load losses equal to 0.4 %. To overcome the absence of DRESs/DBESSs in the original network configurations, 35 and 64 PVs/DBESSs are added in the MV and LV sub-grids, respectively. All DBESSs provide PS and are divided into two groups based on whether they have VR/VUM capability (BT2) or not (BT1). It is worth mentioning that BT2 are placed at the most distant network nodes since they are prone to voltage violations/asymmetries. Details regarding the synergistic implementation of the examined control schemes as well as the connection node and the installed capacity of the PVs/DBESSs are provided in [23]. Finally, the minimum/maximum voltage limits are set to 0.95/1.05 pu for the MV sub-grid and 0.9/1.1 pu for the LV sub-grid.

Concerning the examined PS algorithms, the following parameters are considered: (a) the proportional gain k is set to 2, (b) $RR_{\min}$ and $RR_{\max}$ of the RRL method are set to $-0.0015PV_{\mathrm{cap}}$ kW/s and $+0.0015PV_{\mathrm{cap}}$ kW/s, respectively, where PV_{cap} is the installed capacity of each PV unit, (c) the length of the moving window ($N\Delta\tau$) in the MA technique is 50 s and (d) the time constant of the LPF (T_{lpf}) is equal to 615 s. Furthermore, in both VUM implementation, the damping conductance/susceptance is 1 pu. Note that, VUM is applied only to the unbalanced, due to the connection of single-phase loads, LV sub-grid. Finally, the voltage thresholds (in pu) for the $Q(V)-P(V)$ droop control scheme applied to the MV sub-grid are $[0.95, 0.96, 0.96, 0.97, 1.03, 1.04, 1.04, 1.05]$ [14]. Regarding the LV sub-grid, the solution proposed in [5] is adopted combining a $P(V)$ droop control with the VUM. The voltage thresholds (in pu) of this droop control scheme are $[1.07, 1.09, 1.1]$.

The simulation period is considered one day with time resolution of 1 min. The LV and MV load demand profiles are derived from [15] and [24], respectively. Two types of

simulations are performed assuming generation profiles for a sunny and a cloudy day [25].

IV. Numerical Results

Scope of this section is to discuss and analyze the main outcomes derived from the quasi-static simulations. The analysis is divided into three main parts which are presented in the following subsections.

A. MV-LV Interaction

This subsection investigates the impact of the VR, and specifically of PIC, on the performance of the MV-LV network in terms of maintaining the voltages within the permissible limits. Assuming the sunny day case, the following scenarios are examined: PIC is applied to: (a) MV sub-grid, (b) LV sub-grid, and (c) overall distribution network (both MV and LV sub-grids). The corresponding voltage profiles for two indicative network nodes are depicted in Fig. 2.

According to Figs. 2a and 2b, it can be observed that the activation of the PIC method in only one sub-grid (i.e., either the MV or the LV) cannot efficiently address voltage violations in this part of the network, let alone in the sub-grid where the PIC is deactivated. For example, let us assume the activation of the PIC only in the LV sub-grid. As shown in Fig. 2b, overvoltages at the LV nodes continue to exist even after the activation of the PIC method. This is attributed to the fact that the available active/reactive power of the PVs/DBESSs is not sufficient to tackle overvoltages in this sub-grid. The same conclusion can be drawn when the PIC is applied only to the MV sub-grid, as verified in Fig. 2a. On the contrary, in case the PIC method is applied to both MV and LV sub-grids, the actions taken from the PVs/DBESSs for the VR of one sub-grid, contribute also to the VR of the other sub-grid. As a result, the network voltages are maintained within the permissible limits as shown in Fig. 2c.

From the above, it can be inferred that additional investments in active/reactive power availability from the PVs/DBESSs can be deferred in case a cooperative procedure is adopted towards VR on both MV and LV sub-grids. Additionally, this analysis highlights the need to consider both grid levels when investigating the performance of VR methods, since more accurate and realistic results can be obtained by taking into account the interaction between MV and LV sub-grids. Note that, similar conclusions can be drawn when the PC is applied for the VR of the MV-LV network.

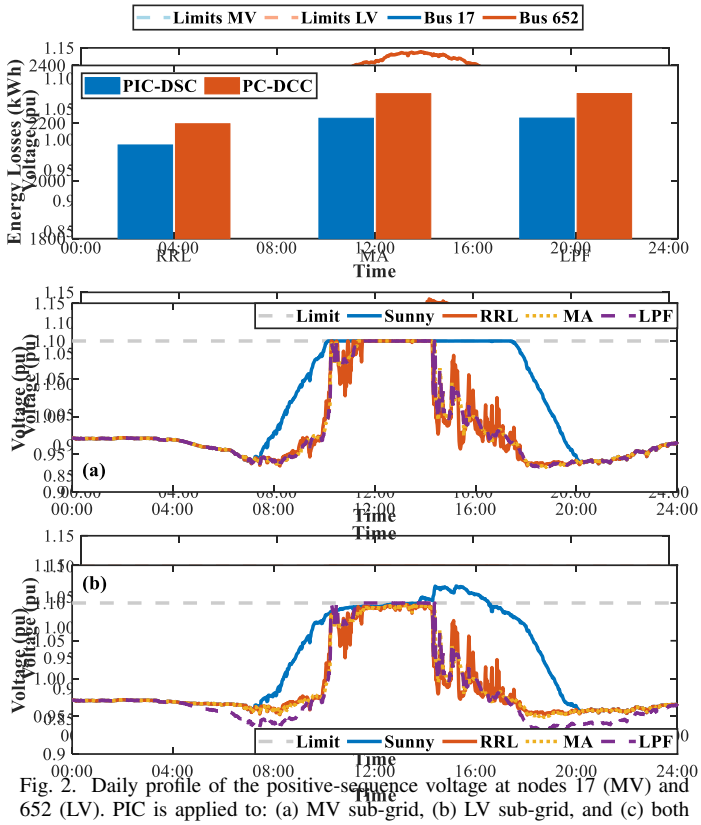

Fig. 2. Daily profile of the positive-sequence voltage at nodes 17 (MV) and 652 (LV). PIC is applied to: (a) MV sub-grid, (b) LV sub-grid, and (c) both MV and LV sub-grids.

Section B

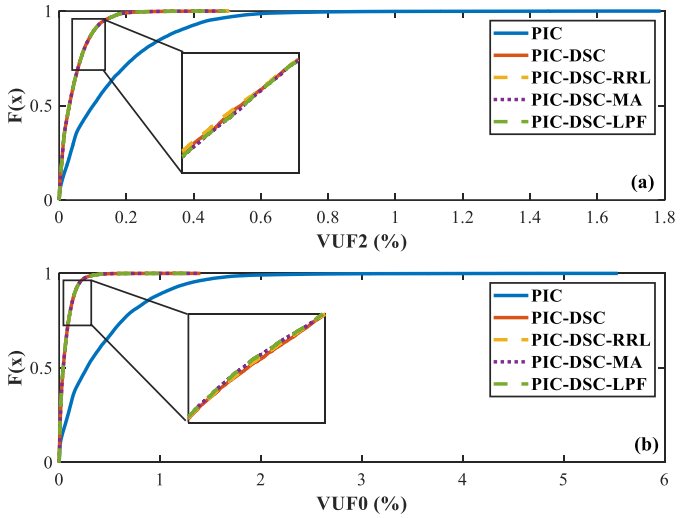

Fig. 3. Cumulative distribution function. (a) VUF2 and (b) VUF0.

B. Provision of Multi-Services

In this subsection, the concurrent operation of the VR, VUM, and PS control schemes is investigated for the cloudy day case. The PIC and DSC schemes are used for VR and VUM of the MV-LV network. The adopted PS control schemes are the LPF, the MA, and the RRL methods. Note that, according to [6], the performance of the PIC method is not influenced by the DSC method and vice versa, since they are fully decoupled due to their implementation in the symmetrical components domain. As a result, only the impact of PS control schemes on the VUM and VR of the MV-LV network is examined in this study.

Concerning VUM, the cumulative distribution function of the negative- (VUF2) and zero-sequence voltage unbalance factors (VUF0) of the LV sub-grid voltages for all the examined combinations of control techniques are presented in Fig. 3. It can be observed that PIC control scheme leads to the highest network asymmetries. On the contrary, the activation of the DSC (PIC-DSC scenario) reduces significantly VUF0 and VUF2. Furthermore, PS activation does not affect the

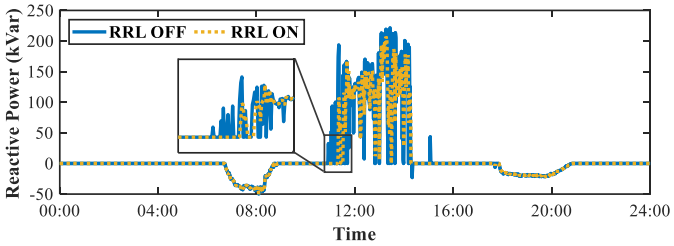

Fig. 4. Daily reactive power profile of the DBESS located at node 16 (MV).

Section A

TABLE I
IMPACT OF MULTI-SERVICES PROVISION ON THE REACTIVE ENERGY USAGE (KVARH)

	PIC	PIC-DSC	PIC-DSC-RRL
MV Sub-grid	2739.88	2739.12	2606.51
LV Sub-grid	381.08	381.22	388.58

TABLE II
IMPACT OF MULTI-SERVICES PROVISION ON THE $wBUI$ OF DBESSS

	PIC	PIC-DSC	PIC-DSC-RRL
MV Sub-grid	≃0	≃0	72.96
LV Sub-grid	0.36	0.36	33.00

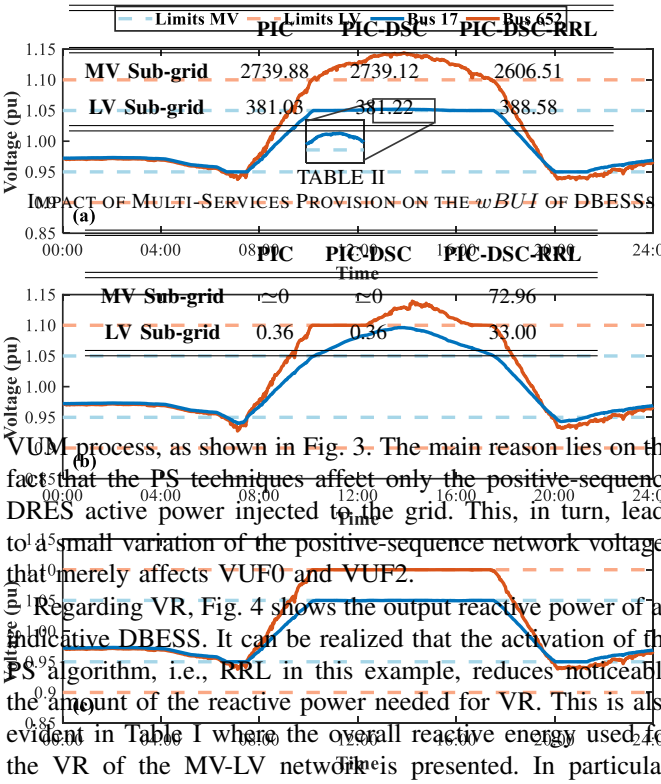

VUM process, as shown in Fig. 3. The main reason lies on the fact that the PS techniques affect only the positive-sequence DRES active power injected to the grid. This, in turn, leads to a small variation of the positive-sequence network voltages that merely affects VUF0 and VUF2.

Regarding VR, Fig. 4 shows the output reactive power of an indicative DBESS. It can be realized that the activation of the PS algorithm, i.e., RRL in this example, reduces noticeably the amount of the reactive power needed for VR. This is also evident in Table I where the overall reactive energy used for the VR of the MV-LV network is presented. In particular, the concurrent operation of VR, VUM, and PS algorithms reduces the overall reactive energy by 4.01 % compared to the case the PS is not used, indicating that the introduction of PS algorithms can lead to a more efficient VR in terms of required reactive energy. However, the activation of the RRL leads to increased DBESS utilization, as shown in Table II, where the weighted DBESSs utilization index ($wBUI$) of [6] is used to quantify the energy provided/stored by all DBESSs as a percentage of the total installed DBESS capacity. From Tables I and II, the decoupling between PIC and DSC is also evident, as both the DBESS utilization and the overall used reactive energy are not influenced by the activation of the DSC.

C. Comparative Assessment of Control Schemes

In this subsection, a comparative analysis is performed to assess the presented data-driven control schemes, in terms of VR, network losses, DBESS utilization, etc., assuming both a cloudy and a sunny day. Specifically, the PIC-DSC solution proposed in [6] is compared with respect to the PC-DCC

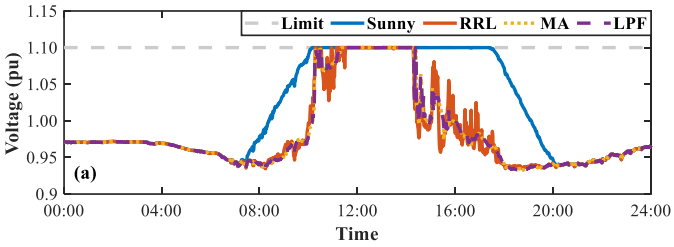

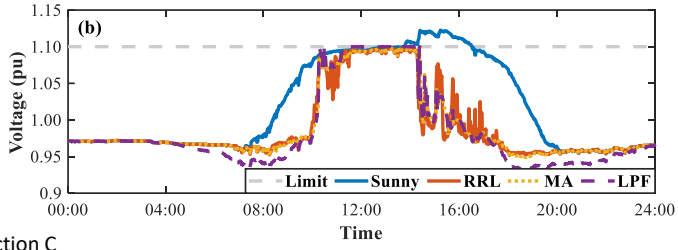

Fig. 5. Daily profiles of the positive-sequence voltage at node 652 (LV). (a) PIC-DSC and (b) the PC-DCC schemes.

Section C

Section B

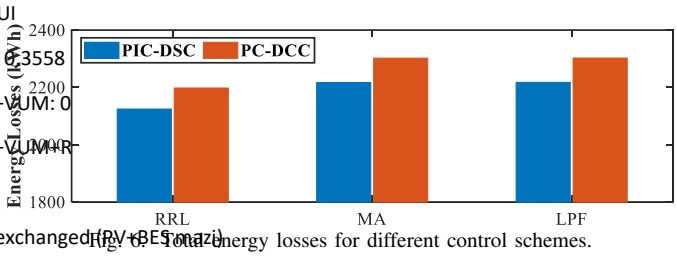

Fig. 6. Total energy losses for different control schemes.

scheme proposed in [5] assuming also the concurrent operation of three different PS algorithms, i.e., RRL, MA, and LPF. Note that, PS techniques are examined considering a cloudy day. The daily voltage profiles of an indicative network node and the network losses are presented in Figs. 5 and 6, respectively. Moreover, the weighted DBESSs utilization index, ($wBUI$) and the overall reactive energy used for VR are shown in Tables III and IV.

The PIC-DSC scheme outperforms the PC-DCC scheme in terms of VR, network losses, DBESS utilization, and reactive energy used for VR. This is an inherent drawback of the PC schemes and especially of the $Q(V)$, $P(V)$ droop control schemes, since the reactive/active power control is activated before reaching the corresponding permissible limits. Therefore, high amounts of unnecessary reactive power flow within the MV-LV network that significantly increase the network losses compared the PIC-DSC scheme, as shown in Fig. 6. Additionally, according to Table III, it can be observed that the DBESS utilization is also increased due to the use of droop control schemes, jeopardizing the VR process. This can be also substantiated from Fig. 5b, where the overvoltages cannot be addressed in case of a sunny day since the corresponding DBESSs have reached their maximum storing capability limits. Finally, among the examined PS techniques, RRL leads to the lowest DBESS utilization and reactive energy usage for both PIC-DSC and PC-DCC schemes, are shown in Tables III and IV, respectively.

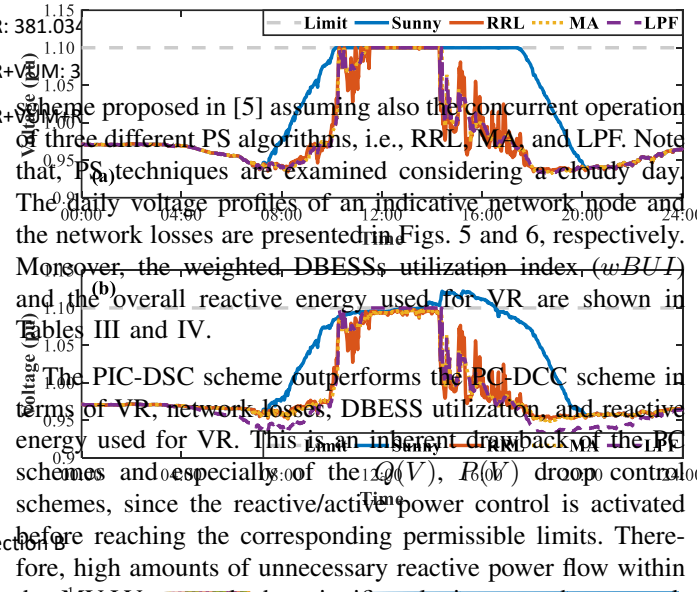

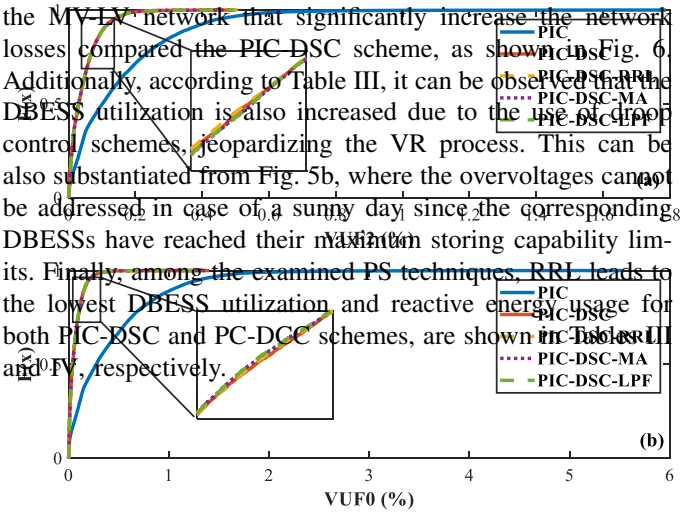

TABLE III
IMPACT OF DIFFERENT CONTROL SCHEMES ON THE $wBUI$ OF DBESSS

	MV Sub-grid		LV Sub-grid	
	PC-DCC	**PIC-DSC**	**PC-DCC**	**PIC-DSC**
RRL	73.00	72.96	38.93	33.00
MA	188.65	188.64	91.51	84.43
LPF	194.12	194.12	93.91	86.86

TABLE IV
IMPACT OF DIFFERENT CONTROL SCHEMES ON THE REACTIVE ENERGY USAGE (KVARH)

		MV Sub-grid		LV Sub-grid	
		PC-DCC	**PIC-DSC**	**PC-DCC**	**PIC-DSC**
RRL	**DBESS**	2577.13	874.71	0.00	209.85
	PV	7548.96	1731.81	0.00	178.73
MA	**DBESS**	2586.42	910.93	0.00	211.65
	PV	7605.34	1859.91	0.00	180.30
LPF	**DBESS**	2581.67	906.02	0.00	211.26
	PV	7590.79	1853.10	0.00	180.03

V. CONCLUSIONS

In this paper, a comprehensive investigation to assess the impact of the most well-established, data-driven VR, VUM, and PS control strategies in MV-LV distribution networks was conducted. This was attained via quasi-static simulations on a MV-LV distribution network consisting of two benchmark MV and LV sub-grids.

Simulation results revealed a strong interaction between MV and LV when assessing the impact of VR. As a result, it is of high importance to consider both grid levels when investigating the performance of VR methods; this also leads to a more realistic grid behavior when evaluating various control schemes. Additionally, the concurrent operation of PS techniques and VR methods can contribute to a more efficient VR in terms of reducing the required reactive energy at the expense of increasing DBESS utilization. Furthermore, it was identified that the impact of the PS techniques on the performance of the VUM methods is negligible. Finally, it was shown that the DBESS utilization and overall reactive energy used for VR are not influenced by applying the DSC scheme concurrently to the PIC method.

REFERENCES

[1] R. A. Walling, R. Saint, R. C. Dugan, J. Burke, and L. A. Kojovic, "Summary of distributed resources impact on power delivery systems," *IEEE Trans. Power Del.*, vol. 23, no. 3, pp. 1636–1644, 2008.

[2] K. E. Antoniadou-Plytaria, I. N. Kouveliotis-Lysikatos, P. S. Georgilakis, and N. D. Hatziargyriou, "Distributed and decentralized voltage control of smart distribution networks: Models, methods, and future research," *IEEE Trans. Smart Grid*, vol. 8, no. 6, pp. 2999–3008, 2017.

[3] Y. Wang, K. T. Tan, X. Y. Peng, and P. L. So, "Coordinated control of distributed energy-storage systems for voltage regulation in distribution networks," *IEEE Trans. Power Del.*, vol. 31, no. 3, pp. 1132–1141, 2016.

[4] T. T. Mai, A. N. M. Haque, P. P. Vergara, P. H. Nguyen, and G. Pemen, "Adaptive coordination of sequential droop control for PV inverters to mitigate voltage rise in PV-rich LV distribution networks," *Elect. Power Syst. Res.*, vol. 192, p. 106931, 2021.

[5] D. V. Bozalakov, T. L. Vandoorn, B. Meersman, G. K. Papagiannis, A. I. Chrysochos, and L. Vandevelde, "Damping-based droop control strategy allowing an increased penetration of renewable energy resources in low-voltage grids," *IEEE Trans. Power Del.*, vol. 31, no. 4, pp. 1447–1455, 2016.

[6] K. D. Pippi, G. C. Kryonidis, A. I. Nousdilis, and T. A. Papadopoulos, "A unified control strategy for voltage regulation and congestion management in active distribution networks," *Elect. Power Syst. Res.*, vol. 212, 2022.

[7] "IEEE standard for interconnection and interoperability of distributed energy resources with associated electric power systems interfaces," *IEEE Std 1547-2018 (Revision of IEEE Std 1547-2003)*, pp. 1–138, 2018.

[8] X. Lyu, Y. Jia, Z. Xu, and J. Østergaard, "Mileage-responsive wind power smoothing," *IEEE Trans. Ind. Electron.*, vol. 67, no. 6, pp. 5209–5212, 2020.

[9] Q. Jiang and H. Wang, "Two-time-scale coordination control for a battery energy storage system to mitigate wind power fluctuations," *IEEE Trans. Energy Convers.*, vol. 28, no. 1, pp. 52–61, 2013.

[10] N. Kakimoto, H. Satoh, S. Takayama, and K. Nakamura, "Ramp-rate control of photovoltaic generator with electric double-layer capacitor," *IEEE Trans. Energy Convers.*, vol. 24, no. 2, pp. 465–473, 2009.

[11] J. Pegueroles-Queralt, F. D. Bianchi, and O. Gomis-Bellmunt, "A power smoothing system based on supercapacitors for renewable distributed generation," *IEEE Trans. Ind. Electron.*, vol. 62, no. 1, pp. 343–350, 2015.

[12] I. de la Parra, J. Marcos, M. García, and L. Marroyo, "Control strategies to use the minimum energy storage requirement for PV power ramp-rate control," *Solar Energy*, vol. 111, pp. 332–343, 2015.

[13] X. Li, D. Hui, and X. Lai, "Battery energy storage station (BESS)-based smoothing control of photovoltaic (PV) and wind power generation fluctuations," *IEEE Trans. Sustain. Energy*, vol. 4, no. 2, pp. 464–473, 2013.

[14] K. D. Pippi, G. C. Kryonidis, A. I. Nousdilis, and T. A. Papadopoulos, "Assessing the provision of ancillary services considering BES capacity degradation," in *2022 Int. Conf. Smart Energy Syst. Technol. (SEST)*, 2022, pp. 1–6.

[15] "European low voltage test feeder," Apr. 01 2021. [Online]. Available: https://site.ieee.org/pes-testfeeders/resources/

[16] S. Karagiannopoulos, C. Mylonas, P. Aristidou, and G. Hug, "Active distribution grids providing voltage support: The Swiss case," *IEEE Trans. Smart Grid*, vol. 12, no. 1, pp. 268–278, 2021.

[17] A. T. Procopiou and L. F. Ochoa, "Asset congestion and voltage management in large-scale MV-LV networks with solar PV," *IEEE Trans. Power Syst.*, vol. 36, no. 5, pp. 4018–4027, 2021.

[18] L. Gutierrez-Lagos and L. F. Ochoa, "OPF-based CVR operation in PV-rich MV–LV distribution networks," *IEEE Trans. Power Syst.*, vol. 34, no. 4, pp. 2778–2789, 2019.

[19] G. C. Kryonidis, A. I. Nousdilis, K. D. Pippi, and T. A. Papadopoulos, "Impact of power smoothing techniques on the long-term performance of battery energy storage systems," *2021 56th Int. Univ. Power Eng. Conf. (UPEC)*, pp. 1–6, 2021.

[20] R. C. Dugan and D. Montenegro, *Reference guide: The Open Distribution System Simulator*, Technical Report 9.0.0., Electrical Power Research Institute, Washington, DC, 2020.

[21] T. M. Inc., "Matlab version: 9.14.0 (r2023a)," Natick, Massachusetts, United States, 2023a.

[22] M. Baran and F. Wu, "Network reconfiguration in distribution systems for loss reduction and load balancing," *IEEE Trans. Power Del.*, vol. 4, no. 2, pp. 1401–1407, 1989.

[23] T. A. Papadopoulos *et al.*, "Validation of a holistic system for operational analysis and provision of ancillary services in active distribution networks," *Energies*, vol. 16, no. 6, 2023.

[24] National Renewable Energy Laboratory, "Commercial and residential hourly load profiles for all tmy3 locations in the united states," 11 2014. [Online]. Available: https://data.openei.org/submissions/153

[25] S. Dimitra Tragianni, K. O. Oureilidis, and C. S. Demoulias, "Supercapacitor sizing based on comparative study of PV power smoothing methods," in *2017 52nd Int. Univ. Power Eng. Conf. (UPEC)*, 2017, pp. 1–6.